ISSN 2723-6471

Detection of COVID-19 using EfficientnetV2-XL and Radam Optimizer from Chest X-ray Images

Ibrahim Alkore Alshalabi[1], Tawfiq Alrawashdeh[2], Sumaya Abusaleh[3], Malek Zakarya Alksasbeh[4,*], Khalid Alemerien[5], Shorouq Al-Eidi[6], Hamzah Alshamaseen[7]

[1,2,3,4]*Faculty of Information Technology, Al-Hussein Bin Talal University, Ma'an, 71111, Jordan*

[5,6]*College of ICT, Tafila Technical University, Tafila, 66110, Jordan*

[7]*IOTISTIC Solutions Company, Amman,11185 Jordan*

(Received: October 30, 2024; Revised: November 22, 2024; Accepted: December 18, 2024; Available online: March 15, 2025)

Abstract

Automating the detection of the COVID-19 pandemic has become necessary for assisting radiologists and medical practitioners in the diagnosis process. It enables them not only to save time through early diagnosis but also to ensure that they are making more accurate diagnoses. Therefore, this research presents a novel approach for automatically identifying COVID-19 in chest X-ray images by utilizing the EfficientNetV2-XL model in combination with the Rectified Adam optimizer for training. For conducting the experiments, we used the dataset available on Kaggle, known as the COVID-19 Radiography Dataset. The totality of this dataset was 21,165, and it included four patterns: COVID-19, viral pneumonia, lung opacity, and normal cases. The dataset was divided into 80% training and 20% testing. The preprocessing stage included resizing images to 512 × 512 pixels and then applying data augmentation techniques to enhance model robustness. Consequently, a fine-tuned multiclass categorization system was implemented. The proposed system's effectiveness is evidenced by the experimental outcomes, which show a 99.31% accuracy rate and a perfect Area Under the Curve score of 1 for identifying COVID-19. Additionally, the Score-CAM visualization method was utilized to enhance the interpretability of model predictions, identifying key regions within the chest X-ray images that influence the classification outcome. This Localization technique aids healthcare professionals in understanding the reasoning behind the model and confirming the accuracy of the diagnosis. The proposed system outperformed the state-of-the-art models for COVID-19 detection.

Keywords: Multiclass Classification, Deep Learning, EfficientnetV2-XL, Radam, COVID-19, Chest X-ray

1. Introduction

The coronavirus disease 2019 (COVID-19) pandemic has escalated the healthcare burden globally. The lungs are the organs most affected by COVID-19 disease [1]. Chest X-ray imaging (CXRI) of the lung is a standard point-of-care radiographic method for screening and diagnosing COVID-19 owing to its ease and availability [2]. The resources to diagnose the deadly disease, with reverberating consequences for communities already on the brink of survival, would increase with the increased availability, preparedness, promptness, and affordability of diagnosis [3], [4].

Thus, the value of COVID-19 detection from CXRI is undisputed. It manifests as infiltrations that appear mainly in the lower region of the lungs. It differs from other pneumonia patterns; therefore, CXRI was used to assess the severity of the infection [5]. CXRI can save time and act effectively in the fight against COVID-19 [6]. However, CXRI is not specific for COVID-19. The variability in the appearance of the lungs makes interpretation more challenging. Some findings also overlap with the typical findings associated with other viral pneumonia cases [7]. Therefore, accurately and swiftly distinguishing COVID-19 from other lung diseases has become critical in the fight against the pandemic [8]. Consequently, advances in deep learning (DL) made it possible to improve disease detection [9]. DL approaches address the challenge of distinguishing COVID-19 from other lung diseases by using advanced neural network architectures to extract and analyze complex patterns in CXRI [10]. EfficientNetV2-XL is a cutting-edge model of neural networks that classifies images with high accuracy and efficiency [11]. Moreover, coupling DL with optimizers

***Corresponding author: Malek Zakarya Alksasbeh (malksasbeh@ahu.edu.jo)**
DOI: https://doi.org/10.47738/jads.v6i2.512

plays a crucial role in training neural networks effectively [12]. The Rectified Adam (Radam) optimizer is a variant of the Adam optimizer that aims to improve the generalization and convergence speed in DL models [13]. Thus, the integration of EfficientNetV2-XL with the Radam optimizer is expected to establish a robust multi-classification system for the detection of COVID-19, enabling the differentiation between COVID-19 and other lung diseases based on CXRI analysis. EfficientnetV2-XL with the Radam optimizer can handle the complicated patterns and characteristics observed in CXRI for lung diseases. Thus, the objective of this research was to develop a multi-classification system for identifying COVID-19 through the analysis of CXRI.

This study makes several significant contributions to the field of medical diagnostics. Firstly, it successfully implements a multiclass medical diagnostic system using CXRI that incorporates the EfficientnetV2-XL architecture and Radam optimizer to categorize four patterns: normal cases, COVID-19, lung opacity, and viral pneumonia. These four distinct patterns are abbreviated as (CPLN) across this research. Secondly, integrating the EfficientnetV2-XL architecture with the Radam optimizer results in a novel method for multiclass classification in medical imaging. Lastly, the localization of CPLN patterns was determined using the Score-CAM approach. Furthermore, the outputs were visually shown through a heatmap that facilitated data analysis.

It is becoming necessary for medical practitioners to automate the diagnostic process of detecting the COVID-19 pandemic. Since it enables them not only to save time through early diagnosis but also to ensure that they are making more accurate diagnoses. As a result, timely inspection and diagnosis can mitigate the life-threatening nature of lung disorders and enhance the quality of life of affected patients. The remainder of this paper is organized as follows. Section 2 presents related work. Section 3 describes the research materials, and the methodology used. Section 4 discusses and analyzes the model outputs. Section 5 concludes the study and highlights future work.

2. Related Work

The urgent need for reliable and rapid identification of COVID-19 infections has led to the exploitation of deep-learning-based models within the medical imaging community. These models have revealed the ability to expedite the analysis of different medical images while maintaining high performance. This section presents a detailed review of the evolution of deep-learning models utilized for the detection of COVID-19 infections, with an emphasis on the analysis of CXRI.

In various DL applications, explicitly using convolution neural networks (CNNs) in COVID-19 detection, Apostolopoulos and Mpesiana [14] adopted various CNN pre-trained architectures such as Inception, VGG19, MobileNetV2, Inception-ResNetv2, Xception as feature extractors in identifying COVID-19 infection process. The fine-tuned pre-trained model results demonstrated the efficiency of utilizing transfer learning in detecting abnormal X-ray images from small datasets, obtaining an accuracy of 96.78% and a recall rate of 98.66%.

A deep CNN model, dubbed COVID-Net, was developed by Wang and Wong [15] to categorize patient images into three classes: COVID-19, normal, and pneumonia cases. COVID-Net offers significant computational efficiency and architectural simplification compared to other pre-trained deep CNN architectures, such as VGG19 and ResNet-50. The model was evaluated using 13,800 X-ray images from 13,645 individuals. The experimental results for COVID-Net showed that the model achieved a recall rate of 91.00% and a test accuracy of 93.30%.

Narin et al. [16] developed a fine-tuned model using various pre-trained transfer approaches, including ResNet101, ResNet50, InceptionV3, ResNet152, and InceptionResNetV2 with X-ray images, to obtain better prediction performance for four distinct classes: COVID-19, bacterial pneumonia, normal, and viral pneumonia. Based on the performance results, the pre-trained ResNet50 method outperformed the other models by obtaining 98% accuracy on the ChestX-ray8 database.

Ozturk et al. [17] developed a model called DarkNet-19 using the YOLO architecture, which is commonly used for real-time object detection. Their experimental results indicated that DarkNet-19 achieved 98.08% accuracy for binary classification and 87.02% accuracy for multiclass classification.

Almutairi et al. [18] developed a lightweight EfficientNet model to classify X-ray images into various categories including normal, pneumonia, COVID-19, and lung opacity. This study involved testing multiple EfficientNet

architectures, specifically EfficientNet-lite-B0, EfficientNet-elite-B9-V2, and EfficientNet-elite-B9-V3. The experimental results indicated that the EfficientNet-lite-B0 model exhibited superior performance. This architecture demonstrated accuracies of 99% for binary classification and 94.9% for multiclass classification, surpassing the performance of other models.

Halgurd et al. [19] evaluated a modification of both the CNN model and AlexNet architecture using two types of images: X-ray and CT scan. Their results showed that the modified AlexNet and CNN achieved accuracy rates of 98% and 94.1 %, respectively. Furthermore, Turkoglu [20] also introduces the COVIDetectionNet model by employing an AlexNet pretrained architecture. COVIDetectionNet architecture combined AlexNet with the Relief algorithm to extract the most relevant features, which were then used through a Support Vector Machine (SVM) classifier. Notably, COVIDetectionNet demonstrated a high accuracy rate of 99.18%.

In addition, Shervin et al. [21] developed a COVID-19 detection model by fine-tuning various deep CNN pre-trained architectures, such as ResNet18, DenseNet121, ResNet50, and SqueezeNet, with the COVID-Xray-5k dataset. The proposed model was evaluated with an accuracy of 90% and a sensitivity of 98 %. A study by Farooq and Hafeez [22] also utilized a COVID-ResNet model, which was derived from a pre-trained ResNet-50 architecture, to identify COVID-19 patients. The researchers adjusted the dimensions of the image and conducted a range of fine-tuning experiments using ResNet50 architecture to improve COVID-ResNet performance. COVID-ResNet achieved an accuracy rate of 96.23% for multi-classes.

Asif et al. [23] introduced the CoroNet model using the pre-trained Xception. CoroNet was trained on a benchmark dataset derived from two publicly available datasets. The coronet was evaluated by classifying three and four classes, and impressive accuracies of 95% and 89.6% were obtained, respectively. In a similar manner, Mahmud et al. [24] utilized depth-wise dilated convolution to introduce the CovXNet model which was trained on a diverse set of X-ray image classes, followed by an additional fine-tuning process. The model attained a classification rate of 90.3% through the implementation of a stacking algorithm during the testing stage.

Chowdhury et al. [25] employed the pre-trained EfficientNet-B5 model to develop the ECOVNet model to detect COVID-19. The researchers developed a set of adaptive data augmentation techniques and optimized the EfficientNet model to enhance the accuracy of ECOVNet classification. The dataset utilized consisted of 14,914 training samples and 1,579 testing samples. The proposed model demonstrated an accuracy of 97% in categorizing multiple classes.

Likewise, Luz et al. [26] used a pre-trained EfficientNet architecture to develop a deep-learning model for identifying COVID-19 instances. Their research results showed that the proposed model attained an average accuracy of 93.9%.

Naidji et al. [24] enveloped the COVID-EfficientNetB7-Attn model by combining an adapted EfficientNet-B7 architecture with an attention mechanism and SVM classifier. Using the attention mechanism and the SE block at the top of EffecientNetB7 enhanced the extracted deep features and led to better performance in COVID-19 diagnosis. The proposed model achieved a recall rate of 100% and an average accuracy of 97.50 % for COVID-19 detection.

Hussain et al. [25] presented CoroDet, a CNN model designed explicitly for the automated detection of COVID-19 using both CT and CXRI. Developed as a reliable classifier, CoroDet is trained for two, three, and four classes. The classifier achieved an outstanding classification rate of 99.1% for binary classification.

Khobahi et al. [26] combined a CNN with an AutoEncoder model to design a semi-supervised learning approach to distinguish COVID-19 cases from normal cases. Autoencoders were used to extract the infected legions from CXRI, and CNN was used to capture the features and train the classifier. The authors showed that their suggested model achieved an average accuracy of 93.50% on a limited available dataset.

In [27] COVID-CXNet, a hierarchical deep-learning model was presented to identify COVID-19. The CheXNet model was built on a pretrained DenseNet architecture. The COVID-CXNet model was developed using a two-step classification process: initially categorizing the X-ray images into two classes, pneumonia or normal cases, followed by an improved classification of the X-ray images into multiple categories, like COVID-19 cases and both normal cases and pneumonia. The proposed model accomplished an accuracy of 87.8%.

The reviewed studies collectively highlight the significant advancements in applying DL models to detect COVID-19 using CXRI. The diverse methodologies and models ranging from fine-tuned pre-trained architectures like ResNet, VGG19, and EfficientNet to specialized models like COVID-Net and COVIDetectionNet demonstrate the versatility and potential of DL in medical diagnostics. These models have consistently shown high accuracy rates, indicating their reliability and efficiency in identifying COVID-19, viral pneumonia, and other lung conditions. The successful implementation of techniques such as transfer learning, attention mechanisms, and data augmentation has further improved the model's performance. Table 1 presents a comprehensive summary of these previous studies, detailing the various DL models, datasets used, cases, and accuracy performance, and providing a clear summary of the recent state of research in this critical area.

Table 1. Overview of prior research on identifying COVID-19 by applying DL models to CXRI.

Study	Cases	Model Used	Accuracy
Ioannis and Tzani [14]	COVID-19: 224 Pneumonia: 700 Healthy: 504	VGG-19	93.48%
Wang and Wong [15]	COVID-19: 5526 Healthy: 8066	COVID-Net	92.40%
Narin et al. [16]	COVID-19: 50 Non-COVID-19: 50	Deep CNN ResNet-50	98.00%
Halgurd et al. [19]	COVID-19: 85 Non-COVID-19: 85	AlexNet	98.00%
Shervin et al. [21]	COVID-19: 184 Healthy: 5000	ResNet18, ResNet50 SqueezeNet, DenseNet121	90.00%
Ozturk et al. [17]	COVID-19:125 Pneumonia: 500 Healthy: 500	DarkCovidNet	87.02%
Luz et al. [28]	COVID-19: 152 Pneumonia: 5421 Healthy: 7966	EfficientNet-B3	93.90%
Almutairi et al. [18]	COVID-19: 2000 Healthy: 2000 Viral Pneumonia: 1345 Lung opacity: 2000	EfficientNet-lite-B0	94.90%
Farooq and Hafeez [22]	COVID-19: 68 Viral Pneumonia: 4914 Bacterial Pneumonia: 400 Healthy: 800	COVID-ResNet	96.23%
Naidji et al. [24]	COVID-19: 16490 Viral Pneumonia: 5555 Healthy: 8085	EffecientNetB7 Attention mechanism	97.50%
Asif et al.[23]	COVID-19: 290 Healthy: 1203 Bacterial Pneumonia: 660 Viral Pneumonia: 931	Xception	95.00%
mahmud et al. [29]	COVID-19: 305 Viral Pneumonia: 660 Bacterial Pneumonia: 931 Healthy: 1203	CovXNet	90.30%

Turkoglu [20]	COVID-9: 219 Pneumonia: 4290 Healthy: 1583	COVIDetectionNet	99.18%
Chowdhury et al. [25]	COVID-19: 489 Viral Pneumonia: 5459 Healthy: 7966	EfficientNet-B5	97.00%
Hussain et al. [25]	COVID-19: 441 Viral Pneumonia: 400 Bacterial Pneumonia: 400 Healthy: 7170	CoroDet	99.10%
Haghanifar et al. [27]	COVID-19: 1326 Normal: 5000	DenseNet-121	87.88%

3. Material and Methodology

This study introduces a multiclass medical diagnosis system designed to detect CPLN from CXRI images. As shown in figure 1, the proposed system encompasses four stages: datasets, data preprocessing, model building and training, and model output (testing).

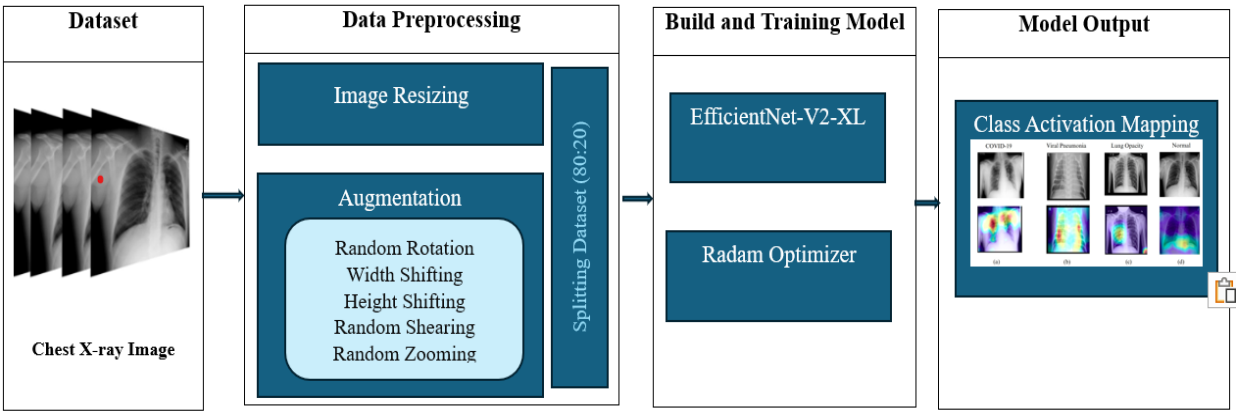

Figure 1. The research methodology

3.1. Datasets

This study used datasets created by a collaborative group of researchers from Qatar University in Doha, Qatar, and the University of Dhaka in Bangladesh, with contributions from colleagues in Pakistan and Malaysia. These researchers developed the COVID-19 Radiography Database, which comprises 3,616 CXRI of COVID-19-positive cases, 6,012 images of lung opacity (non-COVID lung infections), 1,345 images of viral pneumonia, and 10,192 images of normal lungs. Data were extracted directly from Kaggle using the Kaggle API [30].

3.2. Data Preprocessing

The medical image dataset was split into training and test sets, with 80% allocated to the training set and 20% allocated to the test set. This stratification ensured a consistent distribution of classes across both sets. It is worth mentioning that the preprocessing stage of the application under consideration did not incorporate the pixel normalization technique because it is deemed superfluous for certain medical image categorization tasks.

In accordance with the requirements of the CNN, a customized pipeline was implemented to pre-process the image data for the computer vision model. Thus, pre-processing is a two-step approach. First, all the chest X-ray samples were adjusted to a resolution of 512 × 512 pixels. This resolution was chosen to balance the trade-off between computational feasibility and the retention of diagnostically relevant features. Moreover, it ensures that these features are preserved while maintaining compatibility with the EfficientNetV2-XL architecture and the available computational resources. Second, several data augmentation methods were employed to improve the ability of the

model to generalize and reduce overfitting. Data augmentation aims to artificially increase the size of a dataset by producing modified variations in existing observations. Hence, the resilience of the proposed model is enhanced. Therefore, the dataset was augmented for the training phase by using diverse approaches, including random rotation, width and height shifting, shearing, and zooming [2]. These augmentations were specifically employed to introduce realistic variations in the dataset without compromising the integrity of diagnostic features. By increasing the diversity of the training data, these techniques help prevent overfitting and improve the model's performance on unseen data, ensuring clinical applicability.

3.3. Build and Training Model

An optimal architecture and optimizer that reduces the loss function are needed for remarkable image classification performance. This study introduces a deep learning classification model using the EfficientNetV2-XL architecture and Radam optimizer for training.

3.3.1. Employing EfficientNetV2-XL for Extracting Features

CNNs are built with a fixed resource cost and then scaled up to enhance accuracy as resources rise. A standard technique in CNN models includes arbitrarily increasing its depth or width or using a higher-resolution input image for training the model and testing the performance of the model. Although these approaches enhance accuracy, they typically require laborious fine-tuning and nevertheless frequently produce suboptimal performance.

In contrast to the conventional methodologies, EfficientNetV1 architecture was first introduced by M. Tan and Q.V. Le in 2019. The aim was to find a trade-off between accuracy and computing efficiency. Thus, the EfficientNetV1 model applies a compound scaling scheme to adjust the dimensions of the network evenly (width, depth, and resolution). This involves utilizing a user-defined value named (ϕ) that consider the available resources for scaling the model. Hence, simultaneously expanding the network dimensions by a factor of (ϕ) requires approximately $2^{(\phi)}$ times more computing resources. Furthermore, there are eight versions of EfficientNet-V1, denoted as EfficientNetV1-B0 to EfficientNetV1-B7 [31].

EfficientNetV2 was subsequently introduced in [11]. EfficientNetV2 differs significantly from EfficientNetV1 in several key respects. First, EfficientNetV2 heavily utilized both MBConv and Fused-MBConv, particularly in the early layers. As shown in figure 2, the distinction between Fused-MBConv and MBConv lies in the use of Conv3 × 3 ordinary convolution in Fused-MBConv, which replaces the depth-wise Conv3 × 3 depth convolution and Conv1 × 1 convolution in MBConv. Second, EfficientNetV2 prioritizes smaller expansion ratios for MBConv because of its tendency to result in a lower memory access overhead. Third, EfficientNetV2 employs smaller 3 × 3 kernel sizes, while incorporating additional layers to compensate for the reduction in the receptive field resulting from the decreased kernel size. Finally, EfficientNetV2 eliminates the final stage with a stride-1 present in the original EfficientNet, potentially due to its substantial parameter size and the associated complexity of memory access.

Furthermore, the EfficientNetV2 model was optimized by utilizing a training-aware Neural Architecture Search (NAS) and implementing progressive training with an adaptively adjusted regularization approach [11]. This accelerated the training process. Hence, the Efficient-NetV2 model surpasses earlier models in terms of performance while being significantly faster and more parameter-efficient. EfficientNetV2-XL architecture was employed in this study.

 ISSN 2723-6471

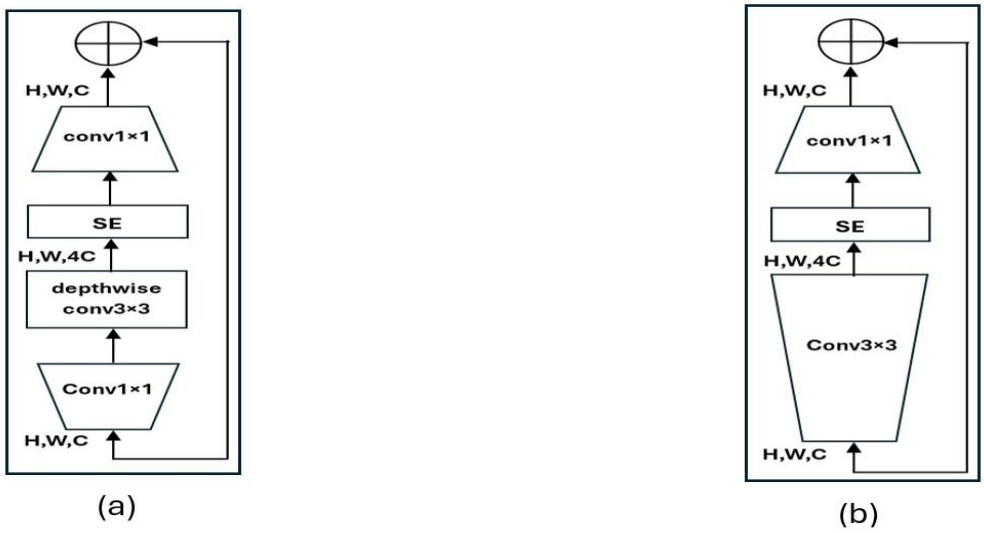

Figure 2. (a) MBConv structure and (b) Fused-MBConv structure [11].

This study employs the EfficientNetV2-XL model [11], which consists of seven blocks, as illustrated in figure 3. The architecture begins with a convolutional layer that includes 32 channels, utilizes a 3 × 3 filter, and operates with a stride of two. A series of Fused-MBConv layers were employed, incorporating different filter sizes, strides, and channels to systematically extract intricate information from the input images. The fused-MBConv1×4 layer operates with a stride of 1 and consistently utilizes 32 channels across the four layers, ensuring accurate feature extraction.

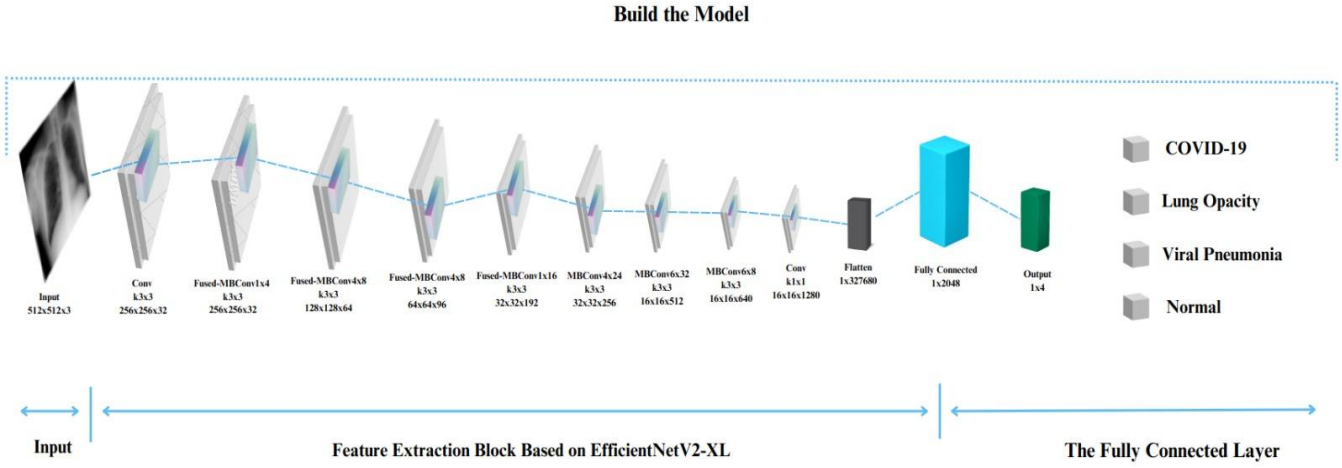

Figure 3. The EfficientNetV2-XL architecture

As the network architecture deepens, it integrates Fused-MBConv layers characterized by increased strides and a greater number of channels, including the Fused-MBConv4x8 and Fused-MBConv1x16 layers. This enhances the capacity of the model to understand complex characteristics. Subsequently, the MBConv layers are utilized, starting with MBConv4x24 and progressing to MBConv6x32, therefore augmenting the feature maps by increasing both the depth and channel dimensions. This was followed using a 1 × 1 convolutional layer with 1280 channels.

Consequently, the feature maps are flattened into a one-dimensional vector of 327680 components, which are fed into a fully connected layer of 2048 neurons, which in turn are connected to an output layer consisting of four neurons representing CPLN cases. Table 2 lists the details of each block structure, including the block number, operator, stride, resolution, number of channels, and number of layers.

Table 2. The structure of EfficientNetV2-XL [11]

Stage	Block	Operator	Stride	Resolution	#Channels	#Layers
Input		-	-	512x512	3	-
Stage 1		Conv3x3	2	256x256	32	1
Stage 2	1	Fused-MBConv1x4	1	256x256	32	4
Stage 3	2	Fused-MBConv4x8	2	128x128	64	8
Stage 4	3	Fused-MBConv4x8	2	64x64	96	8
Stage 5	4	Fused-MBConv1x16	2	32x32	192	16
Stage 6	5	MBConv4x24	2	32x32	256	24
Stage 7	6	MBConv6x32	2	16x16	512	32
Stage 8	7	MBConv6x8	1	16x16	640	8
Stage 9		Conv1x1	1	16x16	1280	1
Stage 10		Fully Connected	-	1x1	2048	1
Output		Fully Connected	-	1x1	4	1

The EfficientNetV2-XL architecture uses a combination of MBConv and Fused-MBConv layers as the primary building blocks [11]. These layers were optimized to handle the complex patterns found in medical images, ensuring robust and accurate diagnoses. Figure 4 illustrates the structures of both Fused-MBConv and MBConv networks.

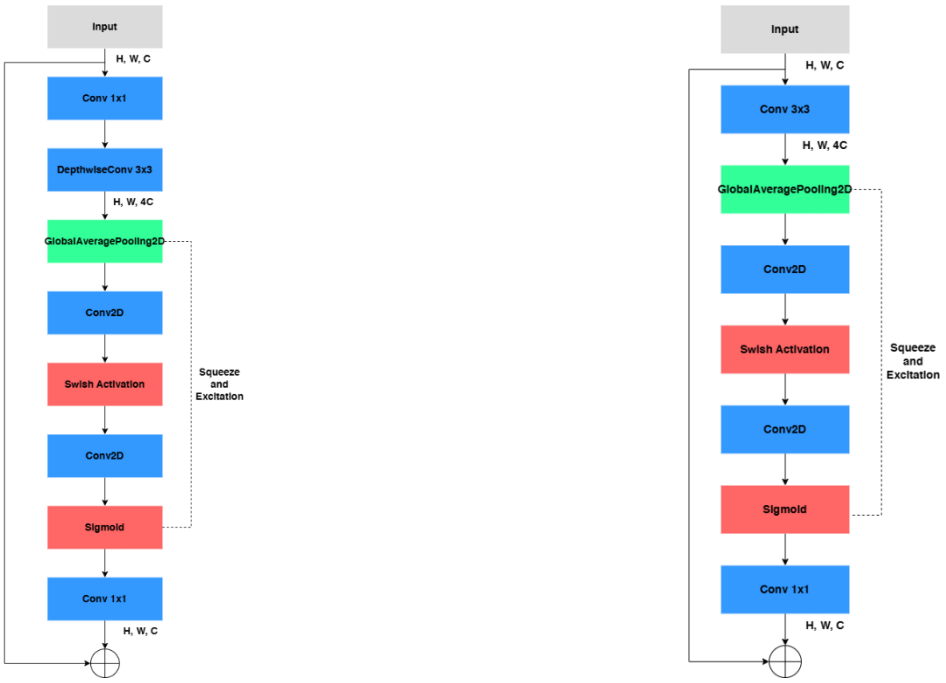

(A) (B)

Figure 4. Structure of (A) MBConv, and (B) Fused-MBConv

Figure 4(a) illustrates MBConv1, whereas figure 4(b) presents Fused-MBConv, both representing distinct design points in the EfficientNetV2-XL architecture [11]. The MBConv block begins with a 1 × 1 convolution followed by a depth-wise 3 × 3 convolution. The output dimensions change from H, W, C to H, W, and 4C after depth-wise convolution. A global average pooling layer reduces the spatial dimensions, followed by a 2D convolution and Swish activation function. Another 2D convolution and sigmoid activation function were applied. The squeeze-and-excitation mechanism is used, which adapts the attention of the network to different channels by weighing them. Finally, a 1 × 1

 ISSN 2723-6471

convolution reduces the dimensions to H, W, and C, and the output is added element-wise to the input. In contrast, the Fused-MBConv block starts with a 3 × 3 convolution instead of the initial 1 × 1 and depth-wise convolutions seen in MBConv. Global average pooling, followed by a 2D convolution, Swish activation, another 2D convolution, and sigmoid activation, is applied similarly. The squeeze-and-excitation mechanism is also discussed here. The block concludes with a 1 × 1 convolution that reduces the dimensions back to H, W, and C, and the output is added element-wise to the input. Notably, both blocks employed the squeeze-and-excitation process to enhance the network's capacity to concentrate on meaningful features.

In addition, we aimed to achieve the best performance of the proposed medical image classification application. The pretrained EfficientNetV2-XL model was fine-tuned on the ImageNet21k-ft1k benchmark dataset. This dataset offers the advantage of being pre-trained on the large-scale ImageNet21k dataset and further fine-tuned on ImageNet1k, thereby providing a robust foundation for transfer learning to medical image classification. Subsequently, a fully connected layer comprising three neurons and employing Softmax activation was incorporated to adapt the model to the specific classification problem under investigation.

So far, EfficientNetV2-XL requires fewer computational resources relative to its capacity compared to other architectures such as ResNet and Xception. This enables it to process high-resolution images (e.g., 512×512) while maintaining computational feasibility. Moreover, its ability to generalize effectively across classes is enhanced when combined with data augmentation techniques and the Radam optimizer, which mitigates overfitting and improves convergence.

3.3.2. Rectified Adam Optimizer

Rectified Adam is a variant of the Adam optimizer, designed to improve training stability and convergence. It addresses potential issues with Adam's adaptive learning rate by adding a rectification term to reduce the variance. This is particularly convenient during the initial few phases of training when the number of samples is small, which may result in less dependable adjustments to the learning rate [13].

Algorithm 1: Rectified Adam Optimizer [13].

Input: $\{\alpha_t\}_{t=1}^{T}$: step size, $\{\beta_1, \beta_2\}$: decay rate is utilized to compute the moving average and moving second moment, θ_0: initial parameter, $f_t(\theta)$: objective function which is stochastic

Output: θ_t: output parameters

1 $m_0, v_0 \leftarrow 0, 0$
2 $\rho_\infty \leftarrow 2/(1-\beta_2) - 1$
3 **while** $t = \{1, \cdots, T\}$ **do**
4 $\quad g_t \leftarrow \nabla_\theta f_t(\theta_{t-1})$
5 $\quad v_t \leftarrow \beta_2 v_{t-1} + (1-\beta_2) g_t^2$
6 $\quad m_t \leftarrow \beta_1 m_{t-1} + (1-\beta_1) g_t$
7 $\quad \widehat{m_t} \leftarrow m_t / (1-\beta_1^t)$
8 $\quad \rho_t \leftarrow \rho_\infty - 2t\beta_2^t / (1-\beta_2^1$
9 $\quad$ **if** *the variance is tractable, i.e.,* $\rho_t > 4$ **then**
10 $\quad\quad l_t \leftarrow \sqrt{1-\beta_2^1 / v_t}$
11 $\quad\quad r_t \leftarrow \sqrt{\frac{(\rho_t-4)(\rho_t-2)\rho_\infty}{(\rho_\infty 4)(\rho_\infty-2)\rho_t}}$
12 $\quad\quad \theta_t \leftarrow \theta_{t-1} - \alpha_t r_t \widehat{m_t} l_t$
13 $\quad$ **else**
14 $\quad\quad \theta_t \leftarrow \theta_{t-1} - \alpha_t \widehat{m_t}$
15 $\quad$ ***return*** θ_T

The pseudocode of Rectified Adam (Radam) is illustrated in Algorithm 1[13]. The process begins by setting the starting values of the first and second moment vectors, (m_0 and v_0), to zero (Line 1). Then, the maximum length of the estimated Simple Moving Average (SMA), denoted as (ρ_{∞}), is calculated (Line 2). For each time step (t) ranging from 1 to T, the gradients (g_t) are computed in relation to the stochastic objective function (Line 4). Both the second moment estimate (v_t) and the first moment estimate (m_t) are updated (Lines 5-6). This is followed by the computation of the bias-corrected first moment estimate ($\widehat{m_t}$) and the length of the estimated SMA (ρ_t) (Lines 7-8). If the value of ρ_t is greater than 4, which reveals that the variance is tractable, the method calculates the adaptive learning rate (l_t) and the variance rectification term (r_t) (Lines 10-11). It then proceeds to update the parameters (θ_t) with the adaptive

 ISSN 2723-6471

momentum (Line 12). On the other hand, if the value of (ρ_t) is less than or equal to 4, the parameters are updated with un-adapted momentum (Line 14). As a result, the parameters θ_T are returned after finalizing the optimization procedure (Line 15). This approach assists in the stability of training and enhances the convergence of neural networks by adaptively rectifying the variance of parameter updates.

In a broader sense, the Radam optimizer is highly efficient in stabilizing training and enhancing convergence, making it crucial for complicated tasks such as the multiclass categorization of medical datasets. In this study, Radam was used in conjunction with EfficientNetV2-XL to achieve fast learning and precise classification of CPLN based on CXRI. The adaptive characteristics of Radam facilitate the management of data changes, resulting in enhanced generalization and performance in the identification and differentiation of different lung disorders.

4. Model Outputs

This section provides details on the empirical settings and outcomes achieved using the dataset under consideration. Various metrics were utilized to evaluate the classification model's effectiveness. Additionally, the Score-CAM method was applied to provide insights into the model's decision-making processes.

4.1. Experiments Setting

The network was trained on TPU v3-8. All training and testing phases were conducted in the same environment utilizing the Keras DL framework and Python 3.9 programming language. Network training was executed with the hyperparameters delineated in table 3.

Table 3. Hyperparameters

Parameter	Value
Input size	512 × 512 × 3
Batch size	128
Learning rate	1e-3
Optimizer	Radam
Epochs	60
Loss function	Categorical Cross entropy

As depicted in table 3, the hyperparameters for the EfficientNetV2-XL model with Radam optimizer were carefully tuned to optimize performance for detecting COVID-19 from chest X-ray images. An input size of 512×512 was chosen to balance detail preservation and computational efficiency. A batch size of 128 ensured effective GPU utilization while maintaining stability during training. The learning rate of 1e-3 was fine-tuned for rapid convergence, complementing the Radam optimizer's ability to stabilize noisy gradients. Sixty epochs provided sufficient training time, validated by monitoring performance metrics to avoid overfitting. Finally, categorical crossentropy was employed as the loss function to handle the multi-class classification task effectively. This configuration achieved robust training and state-of-the-art detection accuracy.

4.2. Classification Performance Evaluation

This study employs indicators such as Precision (P), Recall (R), Accuracy (A), and F1-score to evaluate the performance of the proposed multiclass medical diagnosis model based on the confusion matrix, as illustrated in figure 5. The confusion matrix provides a detailed analysis of the model's classification performance. This matrix highlights the true positives (TP), false positives (FP), false negatives (FN), and true negatives (TN) for each class. For the COVID-19 class, the model correctly identified 718 cases (TP), with 6 FP and 5 FN, and correctly classified 3504 cases as true negatives (TN), demonstrating high specificity and sensitivity. For the Lung Opacity class, 1186 cases were correctly identified (TP), with 28 FP, 17 FN, and 3002 true negatives (TN), indicating robust differentiation from other classes. In the Normal class, the model achieved 2007 TP, 20 FP, and 31 FN, while accurately classifying 2175 cases as TN. Finally, for the Viral Pneumonia class, the model recorded 265 TP, 3 FP, 4 FN, and 3961 TN, reflecting strong performance in identifying these cases. Overall, the confusion matrix underscores the model's ability to achieve

ISSN 2723-6471

a balanced performance across all classes, effectively addressing the challenges of multi-class classification in chest X-ray diagnostics. The formulations for these evaluation measures are detailed in Equations (1)–(4) [32], [33].

$$P = \frac{TP}{TP+FP} \times 100\ \% \quad (1)$$

$$R = \frac{TP}{TP+FN} \times 100\ \% \quad (2)$$

$$A = \frac{TP+TN}{TP+TN+FP+FN} \times 100\ \% \quad (3)$$

$$F1 = 2.\frac{PR}{P+R} \times 100\ \% \quad (4)$$

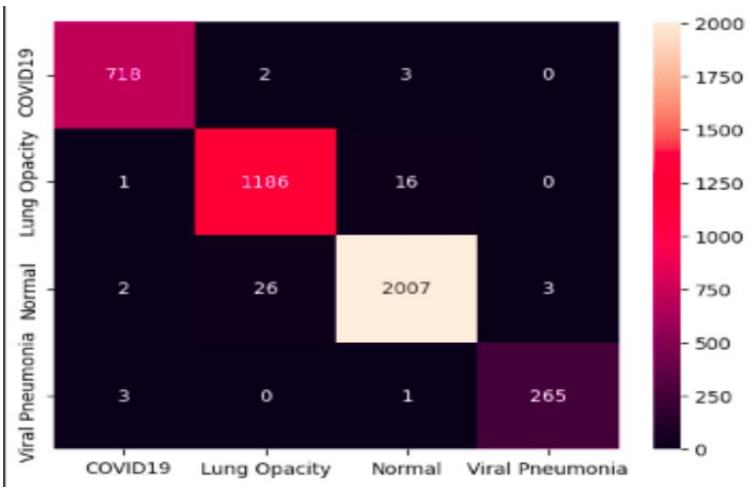

Figure 5. Confusion matrices for CXRI.

Table 4 presents the multiclass classification results, which demonstrate the capacity of the created system to effectively differentiate among CPLN. The multiclass classification system achieved average values for the following various metrics: precision of 98.69%, recall of 98.72%, F1-score of 98.70%, and accuracy of 98.65%. Especially, the system's accuracy at detecting COVID-19 was 99.31%. These findings clearly show that the proposed categorization method reliably diagnoses CPLN patterns using CXRI.

Table 4. Performance Metrics for multi-class classification of CXRI

Classes	Precision (%)	Recall (%)	F1-score (%)	Accuracy (%)
COVID-19	99.17	99.31	99.24	99.31
Lung Opacity	97.69	98.59	98.14	98.59
Viral Pneumonia	98.88	98.51	98.70	98.51
Normal	99.01	98.48	98.75	98.48
Average	98.69	98.72	98.70	98.65

To comprehensively assess the model's performance across various sensitivity and specificity ranges, we employed a Receiver Operating Characteristic (ROC) curve analysis. As illustrated in figure 6, the ROC curve tool was used to evaluate CPLN medical classes. The dataset used for this analysis consisted of X-ray images obtained in this study.

 ISSN 2723-6471

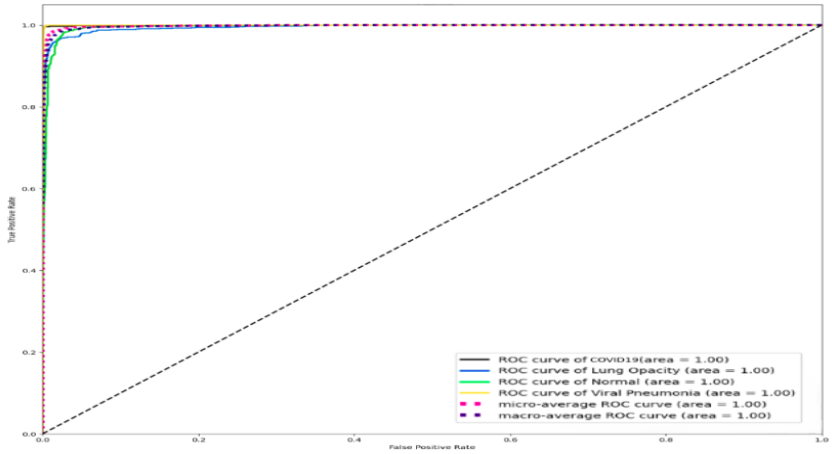

Figure 6. ROC Curves for CPLN patterns using CXRI

The results demonstrated elevated Area Under the Curve (AUC) values, indicating robust model efficiency. The AUC for all classes reached a score of 1.00, signifying perfect separation between the categories of the application at hand and demonstrating the capability of discrimination between dataset samples. The ROC assessments reveal substantial evidence supporting the accuracy of the developed classification system of CPLN patterns under consideration. This also improves the system's capability to deliver precise medical diagnoses through the analysis of the CXRI. Thus, the model can serve as a decision-support tool for healthcare professionals, enabling faster and more precise detection of COVID-19. This capability can streamline diagnostic processes, reduce workload, and ensure timely interventions, particularly in resource-constrained settings or during pandemic surges.

Table 5 provides a comparative analysis of various advanced models utilized for the multiclass categorization task using CXRI to differentiate between the healthy (normal) pattern, the COVID-19 pattern, and other lung disorders patterns under investigation in this study. The proposed EfficientNetV2-XL model demonstrates superior performance compared to state-of-the-art models in terms of accuracy.

Table 5. CXRI comparison of cutting-edge models of deep learning for multiclass classification.

Study	Cases	Model	Accuracy
Luz et al. [26]	COVID-19: 152 Pneumonia: 5421 Healthy: 7966	EfficientNet-B3	93.90 %
Almutairi et al. [18]	COVID-19: 2000 Healthy: 2000 Pneumonia: 1345 Lung opacity: 2000	EfficientNet-lite-B0	94.90 %
Naidji et al. [27]	COVID-19: 16490 Viral Pneumonia: 5555 Healthy: 8085	EffecientNetB7 Attention mechanism	97.50 %
Chowdhury et al. [25]	COVID-19: 489 Viral Pneumonia: 5459 Healthy: 7966	EfficientNet-B5	97.00 %
Proposed	COVID-19: 3616 Viral Pneumonia: 1345 Lung opacity: 6012 Normal: 10192	EfficientNetV2-XL	99.31 %

4.3. Explaining model predictions using Score-CAM

In medical imaging applications, it is essential to enhance the interpretability of deep learning (DL) results. Score-CAM [34] is a powerful method for visualizing the decision on the pattern's label made by deep learning models, emphasizing the areas of an image that significantly impact a specific classification. Score-CAM is typically utilized for diagnostic applications, providing clinicians with an accurate and detailed visualization of the patterns under investigation. This will result in timely medical intervention, thereby enhancing the probability of effective treatment and increasing patient survival rates.

In view of that, the Score-CAM algorithm was employed to evaluate the classification behavior of the proposed model (figure 7). Heatmaps were overlaid on the X-ray image dataset to generate class activation maps, which highlighted areas of significance for differentiating CPLN cases. Analysis of the heatmaps from the Score-CAM algorithm demonstrated that our model could successfully detect regions with bifocal and multifocal glassy opacity (GGO). Notably, the heatmaps of COVID-19-infected images revealed distinct peripheral and diffuse distributions and vascular thickening of the opacity. This localized information can provide clinicians with valuable insights into the factors underlying COVID-19 infection.

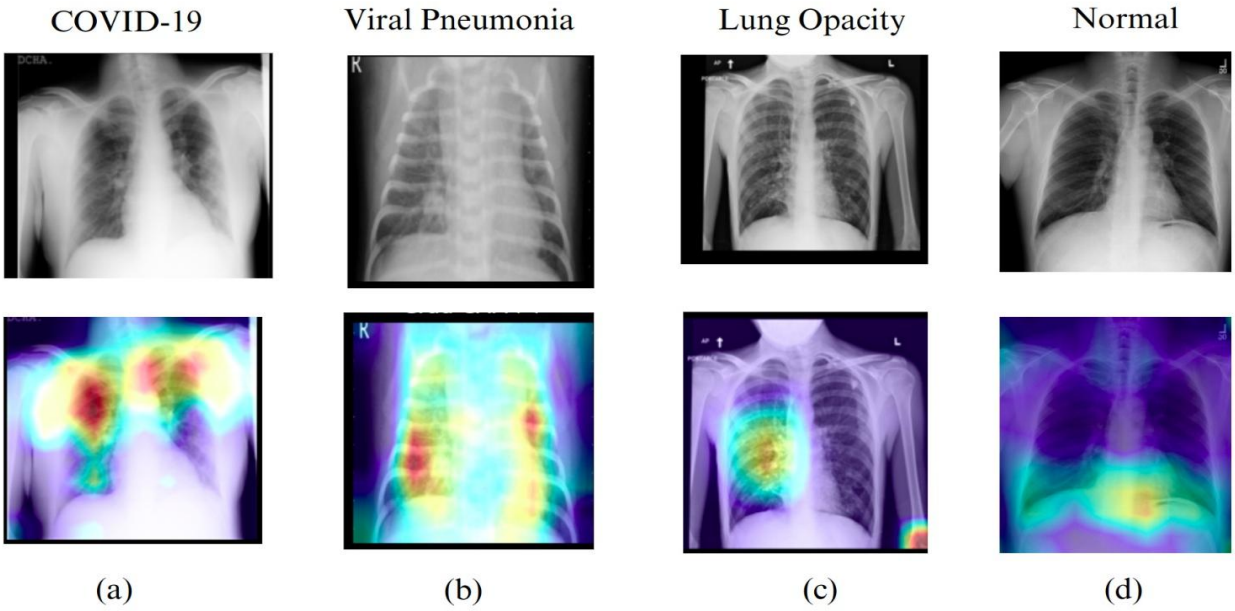

Figure 7. Visualization of chest X-rays using Score-CAM on the Best model. (a) Heatmap for a test image from the COVID-19 class; (b) heatmap for a test image from the Viral Pneumonia class; (c) heatmap for a test image from the Lung opacity case class; (d) heatmap for a test image from the Normal case class.

Figure 7 illustrates Score-CAM visualizations applied to chest X-ray images from the test set using the proposed EfficientNetV2-XL model. The heatmaps highlight regions most influential in the model's classification decisions for the four target classes: (a) COVID-19, (b) Viral Pneumonia, (c) Lung Opacity, and (d) Normal.

For the COVID-19 class (a), the heatmap shows pronounced activation over bilateral lung fields, particularly in peripheral regions, aligning with typical radiographic findings such as ground-glass opacities. In the Viral Pneumonia case (b), the activation is concentrated in lower lung fields, consistent with patchy consolidations. The Lung Opacity class (c) demonstrates central and dense activation correlating with areas of consolidation, while the Normal case (d) exhibits uniform and minimal activation across the lungs, reflecting the absence of abnormalities.

These visualizations enhance the interpretability of the model by correlating its predictions with clinically relevant radiographic features, supporting its integration into diagnostic workflows and increasing confidence in its reliability for real-world clinical applications.

5. Conclusion

This paper presents a robust and accurate DL-based system for the multiclass classification of CPLN from CXRI. By leveraging the EfficientNetV2-XL architecture and Rectified Adam optimizer, our model achieved an impressive accuracy of 99.31% and an AUC of 1 for COVID-19 detection. The use of Score-CAM visualization further enhances the practicality of the system by providing interpretable heatmaps, allowing healthcare professionals to understand the basis of the model's predictions. These findings contribute to a growing body of research demonstrating the potential of DL in medical image analysis, particularly for automated disease detection.

From a practical standpoint, our proposed system holds significant potential as a reliable and efficient tool for assisting radiologists. Its high accuracy and efficiency support its use as a rapid screening tool for COVID-19, particularly in resource-limited settings. Consequently, using automated systems for diagnostic tasks in the healthcare domain confirms its practicality in real-world scenarios. In this view, by automating the phases of the diagnostic process, the system can alleviate the radiologist's workload, enhance the diagnostic classification rate, and expedite treatment. The vision for future improvements involves testing the developed systems' generalizability and resilience on a bigger, more varied dataset gathered from different regions and demographics.

6. Declarations

6.1. Author Contributions

Conceptualization: I.A.A., T.A., S.A., M.Z.A., K.A., S.A.-E., H.A.; Methodology: S.A.; Software: I.A.A.; Validation: I.A.A., S.A., and H.A.; Formal Analysis: I.A.A., S.A., and H.A.; Investigation: I.A.A.; Resources: S.A.; Data Curation: S.A.; Writing – Original Draft Preparation: I.A.A., S.A., and H.A.; Writing – Review and Editing: S.A., I.A.A., and H.A.; Visualization: I.A.A.; All authors have read and agreed to the published version of the manuscript.

6.2. Data Availability Statement

The data presented in this study are available on request from the corresponding author.

6.3. Funding

The authors received no financial support for the research, authorship, and/or publication of this article.

6.4. Institutional Review Board Statement

Not applicable.

6.5. Informed Consent Statement

Not applicable.

6.6. Declaration of Competing Interest

The authors declare that they have no known competing financial interests or personal relationships that could have appeared to influence the work reported in this paper.

References

[1] T. Acter, N. Uddin, J. Das, A. Akhter, T. R. Choudhury, and S. Kim, "Evolution of severe acute respiratory syndrome coronavirus 2 (SARS-CoV-2) as coronavirus disease 2019 (COVID-19) pandemic: A global health emergency," *Science of the Total Environment*, vol. 730, no. 2020, pp. 1-19, 2020, doi: 10.1016/j.scitotenv.2020.138996.

[2] A. S. Althenayan, S. A. AlSalamah, S. Aly, T. Nouh, and A. A. Mirza, "Detection and classification of COVID-19 by radiological imaging modalities using deep learning techniques: a literature review," *Applied Sciences*, vol. 12, no. 20, pp. 1-30, 2022, doi:10.3390/app122010535.

[3] K. Alemerien, S. Alsarayreh, and E. Altarawneh, "Diagnosing Cardiovascular Diseases using Optimized Machine Learning Algorithms with GridSearchCV," *Journal of Applied Data Sciences*, vol. 5, no. 4, pp. 1539-1552, 2024, doi: 10.47738/jads.v5i4.280.

[4] M. Alksasbeh, and M. Al-Kaseasbeh, "Similarity and Agreement Measures and Their Application in Medical Diagnostic Prediction System," *IEEE Access*, vol. 8, no. 2020, pp. 228685-228692, 2020, doi:10.1109/ACCESS.2020.3046456.

[5] A. M. Tahir, M. E. Chowdhury, A. Khandakar, T. Rahman, Y. Qiblawey, U. Khurshid, S. Kiranyaz, N. Ibtehaz, M. S. Rahman, and S. Al-Maadeed, "COVID-19 infection localization and severity grading from chest X-ray images," *Computers in biology and medicine*, vol. 139, no. 2021, pp. 105002, 2021, doi: 10.1016/j.compbiomed.2021.105002.

[6] V. Gupta, N. Jain, J. Sachdeva, M. Gupta, S. Mohan, M. Y. Bajuri, and A. Ahmadian, "Improved COVID-19 detection with chest x-ray images using deep learning," *Multimedia Tools and Applications*, vol. 81, no. 26, pp. 37657-37680, 2022, doi:10.1007/s11042-022-13509-4.

[7] R. A. Reeves, C. Pomeranz, A. A. Gomella, A. Gulati, B. Metra, A. Hage, S. Lange, M. Parekh, A. Donuru, and P. Lakhani, "Performance of a severity score on admission chest radiograph in predicting clinical outcomes in hospitalized patients with coronavirus disease (COVID-19)," *American Journal of Roentgenology*, vol. 217, no. 3, pp. 623-632, 2020, doi:10.2214/AJR.20.2480.

[8] BabitaVerma, R. K. Verma, and A. Mishra, "An Effective Cost-Sensitive Learning Approach for Detection of COVID-19 with Lung Diseases," Smart Healthcare and Machine Learning, M. A. Chaurasia, P. Balaji and A. C. Frery, eds., pp. 79-89, Singapore: Springer Nature Singapore, 2024, doi: 10.1007/978-981-97-3312-5_6.

[9] K. R. Bhatele, A. Jha, D. Tiwari, M. Bhatele, S. Sharma, M. R. Mithora, and S. Singhal, "Covid-19 detection: A systematic review of machine and deep learning-based approaches utilizing chest x-rays and ct scans," *Cognitive Computation*, vol. 16, no. 4, pp. 1889-1926, 2024, doi: 10.1007/s12559-022-10076-6.

[10] A. Ali, Y. Wang, and X. Shi, "Detection of multi-class lung diseases based on customized neural network," *Computational Intelligence*, vol. 40, no. 2, pp. 12649-12668, 2024, doi:10.1111/coin.12649.

[11] M. Tan, and Q. Le, "EfficientNetV2: Smaller Models and Faster Training," in Proceedings of the 38th International Conference on Machine Learning, 2021, vol. 139, no. 1, pp. 10096-10106.

[12] A. AbuKaraki, T. Alrawashdeh, S. Abusaleh, M. Z. Alksasbeh, B. Alqudah, K. Alemerien, and H. Alshamaseen, "Pulmonary Edema and Pleural Effusion Detection Using EfficientNet-V1-B4 Architecture and AdamW Optimizer from Chest X-Rays Images," Computers, Materials and Continua, vol. 80, no. 1, pp. 1055-1073, 2024. doi: 10.32604/cmc.2024.051420.

[13] L. Liu, H. Jiang, P. He, W. Chen, X. Liu, J. Gao, and J. Han, "On the variance of the adaptive learning rate and beyond," *in The Eighth International Conference on Learning Representations(ICLR 2020)*, vol. 2020, no. 1, pp. 1-14, 2020. doi:10.48550/arXiv.1908.03265.

[14] I. D. Apostolopoulos, and T. A. Mpesiana, "Covid-19: automatic detection from x-ray images utilizing transfer learning with convolutional neural networks," *Physical and engineering sciences in medicine*, vol. 43, no. 2020, pp. 635-640, 2020, doi:10.1007/s13246-020-00865-4.

[15] L. Wang, Z. Q. Lin, and A. Wong, "Covid-net: A tailored deep convolutional neural network design for detection of covid-19 cases from chest x-ray images," *Scientific reports*, vol. 10, no. 1, pp. 19549-19572, 2020. doi: 10.1038/s41598-020-76550-z.

[16] A. Narin, C. Kaya, and Z. Pamuk, "Automatic detection of coronavirus disease (covid-19) using x-ray images and deep convolutional neural networks," *Pattern Analysis and Applications*, vol. 24, no. 2021, pp. 1207-1220, 2021, doi:10.1007/s10044-021-00984-y.

[17] T. Ozturk, M. Talo, E. A. Yildirim, U. B. Baloglu, O. Yildirim, and U. R. Acharya, "Automated detection of COVID-19 cases using deep neural networks with X-ray images," *Computers in biology and medicine*, vol. 121, no. 2020, pp. 103792-103821, 2020, doi:10.1016/j.compbiomed.2020.103792.

[18] T. M. Almutairi, M. M. B. Ismail, and O. Bchir, "X-ray Based COVID-19 Classification Using Lightweight EfficientNet," *Journal of Artificial Intelligence* vol. 4, no. 3, pp. 167-187, 2022, doi:10.32604/jai.2022.032974.

[19] H. S. Maghdid, A. T. Asaad, K. Z. Ghafoor, A. S. Sadiq, S. Mirjalili, and M. K. Khan, "Diagnosing COVID-19 pneumonia from X-ray and CT images using deep learning and transfer learning algorithms," in Multimodal image exploitation and learning 2021, 2021, vol. 11743, no. 1, pp. 99-110, doi: 10.1117/12.2588672.

[20] M. Turkoglu, "COVIDetectioNet: COVID-19 diagnosis system based on X-ray images using features selected from pre-learned deep features ensemble," *Applied Intelligence*, vol. 51, no. 3, pp. 1213-1226, 2021.

[21] S. Minaee, R. Kafieh, M. Sonka, S. Yazdani, and G. J. Soufi, "Deep-COVID: Predicting COVID-19 from chest X-ray images using deep transfer learning," Medical image analysis, vol. 65, no. 2020, pp. 101794, 2020, doi:10.1007/s10489-020-01888-w.

 ISSN 2723-6471

[22] M. Farooq, and A. Hafeez, "Covid-resnet: A deep learning framework for screening of covid19 from radiographs," arXiv preprint arXiv:2003.14395, vol. 2020, no. 1, pp. 1-5, 2020, doi:10.48550/arXiv.2003.14395.

[23] A. I. Khan, J. L. Shah, and M. M. Bhat, "CoroNet: A deep neural network for detection and diagnosis of COVID-19 from chest x-ray images," *Computer methods and programs in biomedicine*, vol. 196, no. 2020, pp. 105581, 2020, doi:10.1016/j.cmpb.2020.105581.

[24] M. Rami Naidji, and Z. Elberrichi, "Automatic Detection of COVID-19 from Chest X-Ray Images using EfficientNet-B7 CNN Model with Channel-wise Attention," *International Journal of Computing and Digital Systems*, vol. 15, no. 1, pp. 1443-1456, 2024.

[25] E. Hussain, M. Hasan, M. A. Rahman, I. Lee, T. Tamanna, and M. Z. Parvez, "CoroDet: A deep learning based classification for COVID-19 detection using chest X-ray images," *Chaos, Solitons and Fractals*, vol. 142, no. 2021, pp. 110495, 2021, doi:10.1016/j.chaos.2020.110495.

[26] S. Khobahi, C. Agarwal, and M. Soltanalian, "Coronet: A deep network architecture for semi-supervised task-based identification of covid-19 from chest x-ray images," MedRxiv, vol. 2020, no, 1, pp.1-16, 2020, doi:10.1101/2020.04.14.20065722.

[27] A. Haghanifar, M. M. Majdabadi, Y. Choi, S. Deivalakshmi, and S. Ko, "Covid-cxnet: Detecting covid-19 in frontal chest x-ray images using deep learning," *Multimedia tools and applications*, vol. 81, no. 21, pp. 30615-30645, 2022, doi:10.1007/s11042-022-12156-z.

[28] E. Luz, P. Silva, R. Silva, L. Silva, J. Guimarães, G. Miozzo, G. Moreira, and D. Menotti, "Towards an effective and efficient deep learning model for COVID-19 patterns detection in X-ray images," *Research on Biomedical Engineering*, vol. 38, no. 2022, pp. 149-162, 2021, doi:10.1007/s42600-021-00151-6.

[29] T. Mahmud, M. A. Rahman, and S. A. Fattah, "CovXNet: A multi-dilation convolutional neural network for automatic COVID-19 and other pneumonia detection from chest X-ray images with transferable multi-receptive feature optimization," *Computers in biology and medicine*, vol. 122, no. 2020, pp. 103869, 2020, doi:10.1016/j.compbiomed.2020.103869.

[30] T. Rahman, M. Chowdhury, and A. Khandakar. "COVID-19 Radiography Database," January, 10 2024, 2024; https://www.kaggle.com/datasets/tawsifurrahman/covid19-radiography-database.

[31] M. Tan, and Q. Le, "Efficientnet: Rethinking model scaling for convolutional neural networks," i*n International conference on machine learning*, vol. 2019, no. 1, pp. 6105-6114, 2019.

[32] F. Zhou, S. Hu, X. Wan, Z. Lu, and J. Wu, "Diplin: A Disease Risk Prediction Model Based on EfficientNetV2 and Transfer Learning Applied to Nursing Homes," *Electronics*, vol. 12, no. 12, pp. 1-21, 2023, doi:10.3390/electronics12122581.

[33] H. Al-Mahafzah, T. AbuKhalil, M. Alksasbeh, and B. Alqaralleh, "Multi-modal palm-print and hand-vein biometric recognition at sensor level fusion," *International Journal of Electrical and Computer Engineering (2088-8708)*, vol. 13, no. 2, pp. 1954-1963, 2023, doi:10.11591/ijece.v13i2.pp1954-1963.

[34] H. Wang, Z. Wang, M. Du, F. Yang, Z. Zhang, S. Ding, P. Mardziel, and X. Hu, "Score-CAM: Score-weighted visual explanations for convolutional neural networks," *in Proceedings of the IEEE/CVF conference on computer vision and pattern recognition workshops*, vol. 2020, no. 1, pp. 24-25, 2020